Deep-Learning-Based Pedestrian Inertial Navigation: Methods, Data Set, and On-Device Inference

Changhao Chen, Peijun Zhao, Chris Xiaoxuan Lu, Wei Wang, Andrew Markham, and Niki Trigoni

***Abstract*—Modern inertial measurements units (IMUs) are small, cheap, energy efficient, and widely employed in smart devices and mobile robots. Exploiting inertial data for accurate and reliable pedestrian navigation supports is a key component for emerging Internet of Things applications and services. Recently, there has been a growing interest in applying deep neural networks (DNNs) to motion sensing and location estimation. However, the lack of sufficient labelled data for training and evaluating architecture benchmarks has limited the adoption of DNNs in IMU-based tasks. In this article, we present and release the Oxford Inertial Odometry Data Set (OxIOD), a first-of-its-kind public data set for deep-learning-based inertial navigation research with fine-grained ground truth on all sequences. Furthermore, to enable more efficient inference at the edge, we propose a novel lightweight framework to learn and reconstruct pedestrian trajectories from raw IMU data. Extensive experiments show the effectiveness of our data set and methods in achieving accurate data-driven pedestrian inertial navigation on resource-constrained devices.**

***Index Terms*—Efficient deep learning, Internet of Things (IoT), pedestrian inertial navigation.**

I. Introduction

Modern microelectromechanical system (MEMS) inertial measurement units (IMUs) are small (a few mm^2), cheap (several dollars a piece), energy efficient, and pervasive. As a low-cost yet powerful sensing modality, they have received a large amount of research effort and deeply weave into a wide range of applications. For instance, today's smartphones come with embedded IMUs while users can use them for different location-based services, e.g., indoor navigation, localization, and outdoor trajectory analysis [1]. Moreover, emerging cyber gadgets, such as wristbands and VR/AR headsets, also actively utilize IMUs to provide continuous health monitoring [2], accurate activity tagging [3], and immersive gaming experiences [4]. On the side of robots and autonomous systems, IMUs are a long-standing sensing solution to navigation and grasping tasks [5].

The proliferation of IMUs in the aforementioned applications depends on a method called inertial navigation (also known as intertial odometry). Inertial navigation produces orientation and position of users based on the rotation and acceleration measurements of IMU sensors. Such a method is a pillar to motion sensing, acting as a key enabler for many location-based services. Compared with GPS, vision, radio, or other navigation techniques [6], the inertial solution relies only on self-contained sensor requires few physical infrastructure, and is insensitive to environmental dynamics. This unique property, coupled with the proliferation of IMUs in smart devices, allows the flexibility and reliability to deploy the location service easily to Internet of Things (IoT) applications. Meanwhile, compared with high-dimensional visual data, IMU data are 6-D time series that can be processed in real time even on resource-constrained device. As such, the user's location/motion privacy is thus better protected off the cloud.

To achieve long-term inertial navigation, a major limitation is the unbounded system error growth, caused by various sensor errors and biases due to the use of low-cost IMUs [7]. Most previous work of have exploited the human motion context information to constrain the error drifts of the inertial systems. One solution is to attach the IMU on a user's foot to take advantage of zero-velocity update (ZUPT) for compensating the system drift [8]. Pedestrian dead reckoning systems (PDRs) [1] have been proposed to estimate trajectories by detecting steps and estimating headings. However, these handcrafted algorithms are hard to apply in everyday usage due to the unrealistic assumptions of human motion: ZUPT requires the inertial sensor to be firmly fixed on a user's foot, preventing this solution from being used on consumer devices; PDRs are based on the personal walking models, and constrained only to work under periodic pedestrian motion.

Recently, the deep-learning-based inertial navigation models, e.g., IONet [9], have been proved to be capable of estimating motion and generating trajectories directly from raw inertial data without any handcrafted engineering. Other data-driven methods [10], [11] learn to predict velocities in order to constrain system error drift, and achieve competitive performance. These learning-based models have been shown to outperform the previous model-based approaches in terms of accuracy and robustness [9]–[11]. There is a growing

Manuscript received December 27, 2019; accepted January 9, 2020. Date of publication January 15, 2020; date of current version May 12, 2020. This work was supported in part by Engineering and Physical Sciences Research Council Program Grant Mobile Robotics: Enabling a Pervasive Technology of the Future under Grant GoW EP/M019918/1; and in part by the National Institute of Standards and Technology via the grant Pervasive, Accurate, and Reliable Location-Based Services for Emergency Responders Federal under Grant 70NANB17H185. *(Changhao Chen and Peijun Zhao contributed equally to this work.) (Corresponding author: Chris Xiaoxuan Lu.)*

The authors are with the Department of Computer Science, University of Oxford, Oxford OX1 3QD, U.K. (e-mail: changhao.chen@cs.ox.ac.uk; peijun.zhao@cs.ox.ac.uk; xiaoxuan.lu@cs.ox.ac.uk; wei.wang@cs.ox.ac.uk; andrew.markham@cs.ox.ac.uk; niki.trigoni@cs.ox.ac.uk).

Digital Object Identifier 10.1109/JIOT.2020.2966773

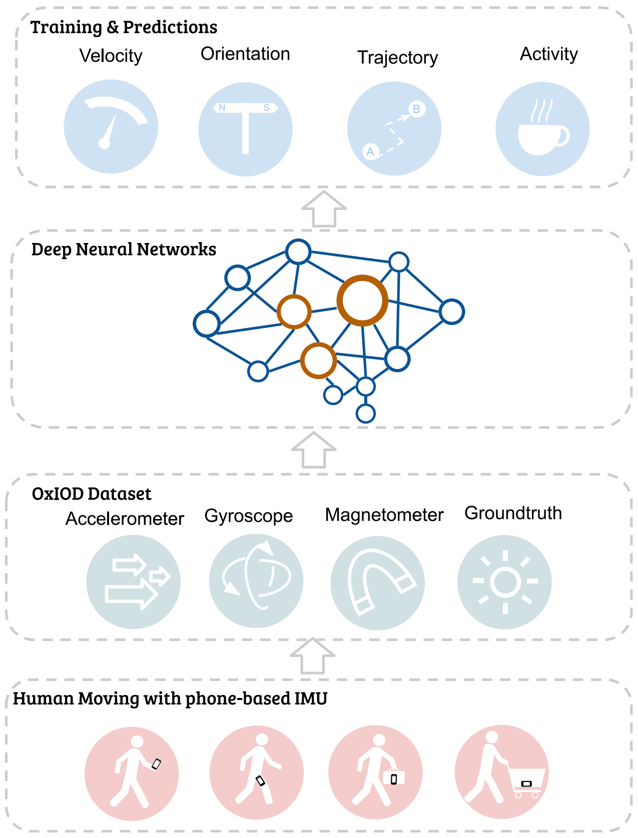

Fig. 1. Deep-learning-based inertial odometry models can learn and predict human motion from raw inertial data.

interest in applying deep neural networks (DNNs) to learn motion from time-series data due to its potential for model-free generalization.

However, to develop the data-driven approaches, we are confronted with the following three main challenges.

1) A significant amount of sensor data with highly precise labels, i.e., the ground-truth values of location, velocity, and orientation, are required for training, validating, and testing the DNN models. Existing data sets [12]–[15] are not suitable for training the DNN models for human tracking, as the sensor data are collected either from vehicles, e.g., cars, or fixed in a specific position, which can not reflect the IMU motion in everyday usage, e.g., as would be sensed by a smartphone.
2) Few works have considered the efficiency of the DNN models for inertial odometry when deployed on low-end devices. It is important for the machine learning models to run at the edge close to where the sensor data are collected, as this will improve the reliability and latency of the inference, and protect the users' privacy [16], particularly in IoT applications.
3) There is a lack of common evaluation benchmarks, whether for conventional PDRs or learning-based models, which precludes a fair and objective comparison of different techniques.

In this article, we present and release the Oxford Inertial Odometry Data Set (OxIOD), with a large amount of pedestrian, multiattachment sensor data (158 sequences, totalling more than 42 km in distance), and high-precise labels, much larger than prior inertial navigation data sets. In order to capture the human motion that accurately reflects everyday usage, the data were collected with a high degree of diversity across different attachments, motion modes, users, and types of device and places. As illustrated in Fig. 1, our proposed data set is able to train the robust and accurate deep learning models for inertial navigation, and we evaluate both the classical algorithms (PDRs) and data-driven models on OxIOD as a common benchmark. To enhance the online efficiency of DNN models on mobile devices, we propose light inertial odometry neural networks (L-IONets), a lightweight DNN framework to learn inertial navigation from raw data without any handcrafted engineering, which is much more efficient at training and inference than previously proposed models using long short-term memory (LSTM) neural network. Extensive experiments were conducted to evaluate the proposed model and existing methods for a systematic study in the performance of the data-driven inertial odometry models in real-world applications and inference at the edge.

In summary, we have three main contributions.

1) We present OxIOD,[1] a first-of-its-kind data set for pedestrian inertial navigation research to boost the adoption of data-driven methods and provide a common benchmark for the task of pedestrian inertial navigation.
2) We propose L-IONet, a lightweight DNN framework to efficiently learn and infer inertial odometry from raw IMU data.
3) We conduct a systematic research in the computational and runtime efficiency of DNN models deployed on low-end mobile devices.

The remainder of this article is organized as follows. Section II surveys the related work on the existing data sets and models. Section III introduces the OxIOD. In Section IV, we present a novel lightweight learning-based inertial odometry model. Section V provides comprehensive evaluations and results.

II. Related Work

A. Inertial Navigation Data Sets

Table I shows representative data sets that include inertial data for the purpose of navigation and localization. In KITTI [12], Oxford RobotCar [13], and EuRoC MAV data sets [17], the sensors are rigidly fixed to the chassis of a car, which is suitable for studying vehicle movements but not directly useful for studying the human movement. The TUM VI data set [14] was collected to evaluate visual-inertial odometry (VIO) with a pedestrian holding the device in front of them. The ground truth in TUM VI is provided at the beginning and ending of the sequences, while during most of the trajectories there is no ground truth. Similarly, in ADVIO [15], the data set is rather short (4.5 km) and only offers pseudo ground truth generated by a handcrafted inertial odometry algorithm.

[1]OxIOD is available at: http://deepio.cs.ox.ac.uk.

TABLE I
COMPARISON OF DATA SETS WITH IMU AND GROUND TRUTH

Dataset	Year	Environment	Attachment	IMU Type	Sample Rate	Groundtruth	Accuracy	Data Size
KITTI Odometry	2013	Outdoors	Car	OXTS RT3003	10 Hz	GPS/IMU	10 cm	22 seqs, 39.2 km
EuRoC MAV	2016	Indoors	MAV	ADIS 16488	200 Hz	Motion Capture	1 mm	11 seqs, 0.9 km
Oxford RobotCar	2016	Outdoors	Car	NovAte SPAN	50 Hz	GPS/IMU	Unknown	1010.46 km
TUM VI	2018	In/Outdoors	Human	BMI 160	200 Hz	Motion Capture	1 mm	28 seqs, 20 km
ADVIO	2018	In/Outdoors	Human	InvenSense 20600	100 Hz	Other Algorithms	Unknown	23 seqs, 4.5 km
OxIOD (Ours)	2018	Indoors	Human	InvenSense 20600	100 Hz	Motion Capture	0.5 mm	**158 seqs**, **42.587 km**

There are several data sets focusing on human gait and activities, which are somewhat similar to our data set, but do not concentrate on localization. Some of these data sets measure human activities, such as USC-HAD [18], CMU-MMAC [19], and OPPORTUNITY [20]. Though these data sets have inertial data with accurate poses as ground truth, they cannot be used to train and test odometry/localisation, since the participants did not move much during the experiments. Some other data sets, such as MAREA [21], focus on human gait recognition and collected inertial data while carriers were walking or running. However, these data sets lack solid ground truth and thus limit their usage in training and testing the odometry models.

As we can see from Table I, our OxIOD data set has a huge amount of data from 158 sequences, leading to a total distance of 42.587 km. The data size of OxIOD is larger than most other inertial navigation data sets, and hence is suitable for DNN methods, which require large amounts of data and high accuracy labels. It should be noted that the total length of the data set even exceeds those collected by vehicles. Meanwhile, our data set can better represent human motion in everyday conditions and thus has a greater diversity.

B. Inertial Navigation Using Low-Cost IMUs

Due to high sensor noise and bias, it is impossible to use conventional strapdown inertial navigation systems (SINSs), which directly integrate inertial measurements into orientation, velocity, and location, on low-cost MEMS IMU platforms. To realize purely inertial pedestrian navigation, most of the existing methods exploit domain-specific knowledge to constrain the error drift of inertial systems. One solution is to attach inertial sensor onto users' foot to take advantage of the stationary phases during human walking to perform the ZUPT. The ZUPT-based method can be further enhanced by known velocity update and double-foot position calibration [22]. Another solution is PDR, which is very common in phone-based pedestrian navigation. Under the assumption that users exhibit periodic motion, PDRs update locations by counting users' steps and estimating their stride length and heading [1]. Recent research focuses on fusing other sensor modalities with the PDR models to further improve the robustness and accuracy, such as wireless signals [23], magnetic fields [24], [25] or UWB [26].

Recent emerging data-driven solutions are capable of learning a more general motion model from a large amount of inertial data without hand-engineering effort. A good example is IONet [9], which proposes to formulate inertial odometry as a sequential learning problem and constructs a deep recurrent neural network (RNN) framework to reconstruct trajectories directly from raw inertial data, outperforming traditional model-based methods. Other methods learn to recover latent velocities [10], [11], or detect more accurate zero-velocity phase, in order to compensate the errors of inertial systems [27]. However, few of the previous works considers the inference efficiency of deep learning approaches when deployed on low-end devices.

TABLE II
OXIOD

	Type	Seqs	Time (s)	Distance (km)
Attachments (iPhone 7P/User 1) (Normally Walking)	Handheld	24	8821	7.193
	Pocket	11	5622	4.231
	Handbag	8	4100	3.431
	Trolley	13	4262	2.685
Motions	Slowly Walking	8	4150	2.421
	Normally Walking	-	-	-
	Running	7	3732	4.356
Devices	iPhone 7P	-	-	-
	iPhone 6	9	1592	1.381
	iPhone 5	9	1531	1.217
	Nexus 5	8	4021	2.752
Users	User 1	-	-	-
	User 2	9	2928	2.422
	User 3	7	2100	1.743
	User 4	9	3118	2.812
	User 5	10	2884	2.488
Large Scale	floor 1	10	1579	1.412
	floor 2	16	2582	2.053
Total		158	53022	42.587

III. OXFORD INERTIAL ODOMETRY DATA SET

This section introduces the OxIOD, a data collection of inertial measurements for training and evaluating the deep-learning-based inertial odometry models. To reflect sensor readings under everyday usage, the data were collected with IMUs with various attachments (handheld, in the pocket, in the handbag, and on a trolley/stroller), motion modes (halting, walking slowly, walking normally, and running), four types of off-the-shelf consumer phones, and five different users, as illustrated in Table II. Our data set has 158 sequences, and the total walking distance and recording time are 42.5 km, and 14.72 h (53022 s).

A. Sensor Setup

The data were collected by the on-board sensors of consumer phones, recording accelerations and angular rates from 6-axis IMUs, and magnetic fields from 3-axis magnetometers. The sensor types of IMUs and magnetometers employed in our adopted mobile phones are listed in Table III. A Vicon motion capture system [28] was deployed to produce high-precise groundtruth values of the object motion, i.e., its orientation,

TABLE III
SENSORS

Mobile Phone	IMU	Magnetometer
iPhone 7 Plus	InvenSense ICM-20600	Alps HSCDTD004A
iPhone 6	InvenSense MP67B	AKM 8963
iPhone 5	STL3G4200DH	AKM 8963
Nexus 5	InvenSense MPU-6515	Asahi Kasei AK8963

velocity, and position. The large-scale collection was conducted on two office floors, where we used a Google Tango Tablet [29] as pseudo ground truth.

IMU: The majority of data were collected with an iPhone 7 Plus device. The IMU inside iPhone 7 Plus is InvenSense ICM-20600, a 6-axis motion tracking sensor. It combines a 3-axis gyroscope and a 3-axis accelerometer. 16-bit ADCs are integrated in both gyroscope and accelerometer. The sensitivity error of the gyroscope is 1%, while the noise is 4mdps/$\sqrt{\text{Hz}}$. The accelerometer noise is 100 $\mu g/\sqrt{\text{Hz}}$.

Magnetometer: The Alps HSCDTD004A embedded in iPhone 7 Plus is a 3-axis geomagnetic sensor, which is mainly used for electronic compass. It has a measurement range of $\pm$1.2mT and an output resolution of 0.3 μT/LSB.

Vicon System: We deployed 10 Bonita B10 cameras in the Vicon motion tracker system [28], encircling an area where we conducted data collection experiments. Each Bonita B10 camera has a frame rate of 250 fps, and resolution of 1 megapixel (1024*1024). The lens operating range of Bonita B10 can be up to 13 m. These features enable us to capture motion data with a precision down to 0.5 mm, making the ground truth very accurate and reliable. The software used in the Vicon system is *Vicon Tracker 2.2*. We connected Vicon tracker to robot operating system (ROS) with *vicon_bridge*, and recorded the data stream with rostopic. The map size of our experimental setup in Vicon room is 5 m $\times$ 8 m.

Time Synchronisation: The IMU and magnetometer are integrated in the mobile phone, sharing the same time stamp. Vicon data recorded with ROS is saved with UTC timestamp. Before each experiment, we synchronized the time of iPhone 7 Plus and ROS with UTC, and thus all time stamps recorded along with sensor data will be synchronized.

B. Data Collection

Attachments: The phone-based IMUs will experience distinct motions when attached in different places. In the context of pedestrian navigation, a natural use of mobile phone leads to an unconstrained placement of inertial sensors, and therefore we selected four common situations to study, i.e., the device is in the hand, in the pocket, in the handbag, or on the trolley. In our data collection, a pedestrian (named User 1) walked naturally inside the Vicon room, carrying a phone in four attachments. Fig. 2 shows in which way the devices were held during the experiments.

Motion Modes: Humans move in different motion modes in their everyday activities. We selected and collected data from four typical motion models: 1) halting; 2) walking slowly; 3) walking normally; and 4) running. The experiments with different motion modes were performed by user 1 with iPhone 7Plus in hand, to reduce the influences from user walking habits or sensor properties. The velocities of participants are around 0.5 m/s, 1 m/s, and 1.5 m/s during slow walking, normal walking, and running. Our experiments indicate that the user speeding can be directly recovered from raw inertial data via DNNs, even under a mixed of motion modes.

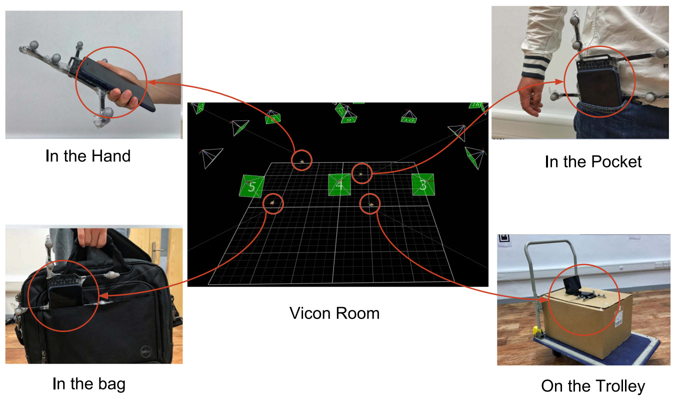

Fig. 2. Inertial data are collected from a smartphone in four different attachments: handheld (left above), pocket (right above), handbag (left below), trolley (right below). The high-precise motion labels are provided by the Vicon system.

Devices and Users: Both the sensors properties and the walking habits of users throw impacts on the performance of inertial navigation systems. In order to ensure inertial odometry invariant across devices and users, we collected data from several types of devices and different users. Four off-the-shelf smartphone were chosen as experimental devices: iPhone 7 Plus, iPhone 6, iPhone 5, and Nexus 5, listed in Table III. Five participants were recruited to perform experiments with phone in the hand, pocket and handbag, respectively. The mixed data from various devices and users can also be applied in the identification of devices and users.

Large-Scale Localization: Besides the extensive data collection inside the VICON room, we also conducted large-scale tracking in two environments. Without the help of Vicon system, Google Tango device was chosen to provide pseudo ground truth. The participant was instructed to walk freely in an office building on two separate floors (about 1650 and 2475 m^2). The smartphones were placed in the hand, pocket and handbag, respectively, while the Tango device was attached on the chest of the participant to capture precise trajectories. Fig. 8(a) and (b) illustrates the floor maps and pseudo ground truth trajectories captured by Google Tango.

IV. Inertial Navigation Models

In this section, we selected and introduced two typical inertial navigation models as our baselines: one is a model-based method, PDR [1], [30], and the other one is a deep-learning-based method, IONets [9]. PDR detects steps, estimates step length and heading and updates locations per step, mitigating exponential increasing drifts of the SINS algorithm into linear increasing drifts. IONet is able to learn self-motion directly from raw data above large data set and solve more general

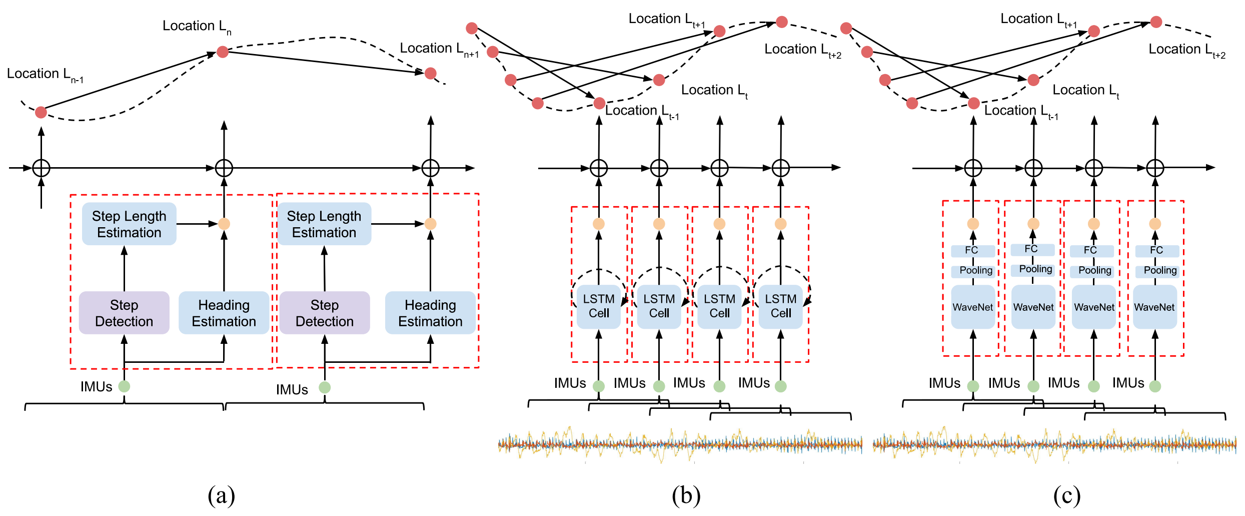

Fig. 3. Framework illustration of three inertial navigation models. (a) PDR. (b) Inertial odometry neural network (IONet). (c) L-IONet.

motion with advantages of extracting high-level motion representation without hand-engineering. A novel lightweight DNN framework, the L-IONets, is proposed to enable more accurate and efficient inference for inertial navigation from low-cost IMU data. Fig. 3 illustrates the frameworks of the PDR, IONet, and L-IONet model.

A. Pedestrian Dead Reckoning

PDRs output pairs of [step length, step heading] to construct 2-D trajectories on a plane. Instead of naively double-integrating inertial measurements, the PDR algorithms detect steps and estimate step length from a duration of classified inertial data using the human walking model. We implemented a basic PDR algorithm to quantitatively evaluate its performance on the OxIOD data set. Aided by the common benchmark, extensions are easy to add on this basic PDR to show the effectiveness of each module.

The PDR models mainly consist of four parts: 1) step detection; 2) step length estimation; 3) heading estimation; and 4) location update. In our PDR model, the step detection thresholds the mean and variance of accelerations, which further classifies the sensory reading into separate independent strides. A dynamical step length estimation module uses the Weinberg's empirical equation [31] to produce the location displacement Δl during a pedestrian stride. Gyroscope signals are integrated into the orientation of inertial sensor, but only the yaw angle is kept as pedestrian heading ψ. The current location (L_k^x, L_k^y) can be updated with the previous location (L_{k-1}^x, L_{k-1}^y) via

$$\begin{cases} L_k^x = L_{k-1}^x + \Delta l \cos(\psi_k) \\ L_k^y = L_{k-1}^y + \Delta l \sin(\psi_k) \end{cases} \tag{1}$$

where Δl and ψ_k are the step length and heading at k th step.

In real-world practice, it is not always easy for the hand-built algorithms to classify inertial data correctly only based on data patterns. Even if the step detection and classification are accurate, the empirical human walking model to estimate step length is highly correlated with user's walking habits and body properties, causing unavoidable accumulative errors during long-term operating.

B. Inertial Odometry Neural Networks

IONets [9] are able to learn user's ego-motion directly from raw inertial data and solve more general motions. For example, tracking a trolley or other wheeled configurations is quite challenging for PDR models, due to the fact that no walking step or periodicity patterns can be detected in this case. In contrast, IONet can regress the location transformation (the average speed) during any fixed window of time, without the explicit components of step detection and step length estimation as in PDRs.

We implemented and trained the IONet model on the OxIOD data set to show the effectiveness of OxIOD for data-driven approaches. The continuous inertial readings are segmented into independent sequences of n frames IMU data $\{(\mathbf{a}_i, \mathbf{w}_i)\}_{i=1}^n$, consisting of 3-D accelerations $\mathbf{a}_i \in \mathbb{R}^3$ and 3-D angular rates $\mathbf{w}_i \in \mathbb{R}^3$ at the time step i. The 6-D inertial data are preprocessed to normalize the accelerations and angular rates into a same scale. The generated sequences are further fed into the RNNs, e.g., LSTMs, to extract effective features for motion estimation. Specifically, Fig. 4(a) illustrates the details of LSTM-based IONet. Each frame of inertial data is used as a input for single LSTM cell: $\mathbf{x}_i = (\mathbf{a}_i, \mathbf{w}_i)$. In the recurrent model, a hidden state $\mathbf{h}_i$ containing the history information of inputs, is maintained and updated at each step i by

$$\mathbf{h}_{i+1} = \mathrm{LSTM}(\mathbf{h}_i, \mathbf{x}_i). \tag{2}$$

This recurrent process compresses the high-dimensional inertial sequence to a high-level compact motion description $\mathbf{h}_i \in \mathbb{R}^m$, where m is the number of hidden states. Finally, after recurrently processing all the data, the last hidden feature $\mathbf{h}_n$ contains the compressed information of the entire sequence for the motion transformation prediction.

In an IONet model, the polar vector $(\Delta l, \Delta\psi) \in \mathbb{R}^2$ (the displacement of location and heading), which proves to be

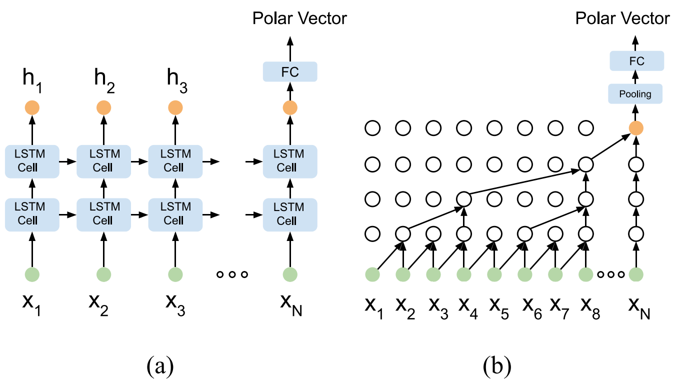

Fig. 4. Comparison of LSTM-based IONet and WaveNet-based L-IONet.

observable from a sequence of inertial data, is learned by LSTMs. After LSTMs, a fully connected layer then maps the hidden features into the target polar vector

$$(\Delta l, \Delta\psi) = \mathrm{FC}(\mathbf{h}_n). \tag{3}$$

Subsequently, in a sequence with timesteps between [0, n], the location (L_n^x, L_n^y) at the nth step is updated by

$$\begin{cases} L_n^x = L_0^x + \Delta l \cos(\psi_0 + \Delta\psi) \\ L_n^y = L_0^y + \Delta l \sin(\psi_0 + \Delta\psi) \end{cases} \tag{4}$$

where (L_0^x, L_0^y) and ψ_0 are the beginning location and heading of the sequence.

Instead of building an explicit model to describe human motion, such as Weinberg's model [31], IONet is able to model motion dynamics and temporal dependencies of sensor data implicitly. Compared with PDR models, IONet is not restricted to the empirical step model, but is capable of regressing the average velocity anytime, i.e., the location transformation during any fixed period of time.

C. Lightweight Inertial Odometry Neural Networks

To this end, we introduce the L-IONet, a lightweight framework to learn inertial tracking, which is more efficient in resource and computational consumption than the previous IONet approach. The detailed structure of L-IONet can be found in Fig. 4(b).

Although deep learning solutions demonstrate great potential to solve sensing problems, e.g., IONet in inertial navigation, their huge computational and memory requirement slows down the deployment of DNN models onto low-end devices [32]. Compared with deploying machine learning models on the cloud, computation at the edge reduces the bandwidth usage, cloud workload, and latency. Besides, it helps protect the users' privacy, as all sensor data hence remain at the users' device rather than uploading to the cloud [16]. Therefore, it is necessary to design an efficient and fast DNN model to enable the inference of IONet on low-end devices, e.g., mobile phone, smartwatch, and Raspberry Pi.

The main bottleneck of IONet framework is the LSTM module. During the backpropagation of model training, recurrent models confront the so-called gradients vanishing problem [33], when processing long sequential data. This is especially the case in our inertial tracking task, as the input is a long sequence of 200 frames of inertial measurements, causing the optimization of recurrent models to be hard and unstable. Moreover, parallel training and inference are difficult for recurrent models, due to the fact that recurrent models have to exploit the sequential relation of the inputs and outputs. This limitation requires a sequence of inputs to be fed into recurrent models in order, consuming huge training time and computational resources to converge. In addition, the inference speed is a bottleneck for deploying RNN models on low-end devices, such as IoT devices or mobile phones, because of the complex operations inside recurrent networks. In contrast, the feed-forward models, e.g., WaveNet, are more lightweight, and able to balance the tradeoff between the accuracy and inference speed [34].

We propose to replace the recurrent model with an autoregressive model to produce outputs using the recent frames of a sequence. A good example is WaveNet, a generative causal autoregressive model, widely applied in processing speech and voice signals for synthesis tasks [34]. Inspired by WaveNet, we propose an autoregressive model-based L-IONet to process the long continuous signals of inertial sensors to predict polar vectors, which are further connected with previous states to reconstruct trajectories. Because L-IONet has no recurrent module and fewer complex nonlinear operations, this feed-forward model is easier to train in parallel, and much faster at state inference.

The basic module of our proposed framework is the causal dilated convolution layer. It can be viewed as a convolutional neural network (ConvNet) with a sliding window, but is a specific type of ConvNet that works perfectly on long sequential data. Compared with a regular ConvNet, the causal convolution inside our model is a 1-D filter that convolves on the elements of current and previous timestep from the last layer, to prevent using future states, as shown in Fig. 4(b). The stacked layers of dilated convolutions allow the receptive area of convolution operation to be made very large by using the convolution that skips input values with a certain distance. Hence, the model is able to capture a long sequence of data without being too huge [35].

Each causal dilated convolution performs via a gated activation unit

$$\mathbf{z} = \tanh\big(\mathbf{W}_{f,k} * \mathbf{x}\big) \odot \sigma\big(\mathbf{W}_{g,k} * \mathbf{x}\big) \tag{5}$$

where $\mathbf{W}$ denotes the weights of the convolutional filters, f and g represent filters and gates, k is the layer index, $*$ is the convolution operator, and $\odot$ is an element-wise multiplication operator. Meanwhile, the residual and skip connection modules are adopted to enable a deeper structure, and improve the model's nonlinearity in regression.

In our L-IONet framework, several layers of dilated causal convolutions are stacked to increase the receptive areas of the inputs. They skip the inputs with a specified stride, and their dilation doubled for every layer. In our case, an 8-layers model with a dilation of 1, 2, 4, 8, 16, 32, 64, and 128 for each layer respectively, is enough to process a sequence of 200 frames of inertial data.

The original WaveNet is designed for audio generation, which quantizes the real data into possible values and reconstructs from the quantized data using the softmax function. Instead of learning classification possibility, our framework replaces the softmax function with a pooling layer and a fully connected layer to map the extracted features $\mathbf{z}$ into the 2-D polar vectors

$$(\Delta l, \Delta\psi) = \mathrm{FC}(\mathrm{Pool}(\mathbf{z})). \quad (6)$$

Similar to IONet model, the predicted polar vectors are further connected with previous system states to produce current locations via (4).

Compared with IONet, the main advantages of our proposed L-IONet can be summarized in twofolds.

1) *Accuracy:* The WaveNet module inside our L-IONet is extremely suitable to processing long continuous sensor signals, i.e., inertial data in our case. Compared with recurrent models, WaveNet mainly consists of dilated causal convolutions, which is easier to optimize, converge, and recover optimal parameters during training, as no hidden states need to be updated and maintained for a long sequence of input data. Besides, the residual modules inside WaveNet further improves the expressive capacity of our model and thus provides more accurate polar vector predictions.
2) *Efficiency:* L-IONet shows a large improvement of both training and inference speed over IONet, enabling it to be deployed onto low-end devices easily, as illustrated in the experiments of Section V. On one hand, WaveNet allows parallel training. On the other hand, the convolutional operations in our L-IONet are faster to perform than the complex operations inside recurrent models [32]. The power of feed-forward models (e.g., WaveNet or Transformers [36]) has already shown a huge improvement in voice synthesis and machine translation [37]. Recently, there is a trend to replace the LSTM module with feed-forward models in sequence modeling tasks. However, few works have explored the potential applications of feed-forward models in processing continuous sensor data, e.g., inertial data as inertial tracking in our case.

D. Sliding Window

In order to increase the output rate of neural network predictions, we present a sliding window method. As Fig. 3(b) and (c) demonstrated, the inertial sensory readings are segmented into independent sequences by using a fixed-size sliding window. In our problem, we choose n the window size of the sequence as 200 frames (2 s), with a stride for sliding the window as 10. The polar vector is predicted by the DNNs from each sequence, and connected by a merging module to generate locations, as described in (3). Note that the current location is updated with the location of 200 frames before it rather than the previous states 10 frames before it. With the predictions from the overlapping windows, the output rate is increased into 10 Hz. Low-pass filters are further used upon the polar vectors and locations to smooth the predictions for trajectory reconstruction.

V. Experiments

In this section, we implemented and trained the IONet and L-IONet models on the OxIOD data set, and conducted extensive experiments to evaluate their performance on the low-end devices, velocity estimation, and localization experiments.

A. Setup

Training and Testing: We split the data set into the training and testing sets for each attachment scenario, i.e., handheld, pocket, handbag, and trolley. The detailed description can be found in the data set folder. All the data are split using a window size of 200 and a stride of 10. Considering the convenience of deploying on devices, our IONet and L-IONet were implemented in the Keras framework with a tensorflow backend. By minimizing the mean square error (MSE) between the estimated values and ground truth provided by our data set, the optimal parameters were trained via the ADAM optimizer [38] with a learning rate of $1e^{-5}$. The batchsize is chosen as 256. We trained each of the model configurations on one NVIDIA TESLA K80.

Devices: To evaluate the performance of our proposed models on low-end devices, we chose three levels of off-the-shelf consumer smartphones, i.e., Huawei Mate 8, Nexus 6, HTC One M8, and one consumer smartwatch, i.e., Sony Smartwatch 2. Huawei Mate 8 is equipped with octa-core (4×2.3 GHz and 4×1.8 GHz) CPU and 4-GB RAM. Nexus 6 is equipped with quad-core 2.7-GHz CPU and 3-GB RAM. HTC One M8 is equipped with quad-core 2.5-GHz CPU and 2-GB RAM. Sony Smartwatch 2 is equipped with 1 core 180-MHz CPU and 256-MB RAM. Our IONet and L-IONet models were first trained with the Keras framework on GPUs, further converted into Tensorflow Lite models, and then deployed on the low-end devices to test their inference speed.

B. Model Performance at the Edge

We conducted a systematic research in the inference performance of DNNs models for inertial tracking at the edge. The LSTM-based IONet is compared with our proposed WaveNet style L-IONet with different hyperparameters chosen to demonstrate their impacts on the model performance, which are the number of layers, whether LSTMs are bi-directional or not, the number of hidden states for LSTMs, and the number of convolutional filters for WaveNet. Moreover, we replaced the LSTM module in IONet with GRUs and Basic RNNs as baselines to show the tradeoff between model accuracy and efficiency.

Fig. 5 compares different model configurations of IONet (LSTM), IONet (GRU), IONet (Basic RNN), and L-IONet (WaveNet), in terms of their number of parameters, training speed, and MSE of predicted polar vectors. It is clear to see that the L-IONet with 32 filters, i.e., WaveNet (32), achieves the highest accuracy with a prediction error of 0.0069, even slightly lower than that of IONet with 1-layer Bi_LSTM (128), i.e., 1-layer Birectional LSTM with 128 hidden states. In contrast, the number of parameters in the L-IONet with WaveNet (32) is only one quarter that of the IONet with 1-layer Bi-LSTM (128). Meanwhile, L-IONet with

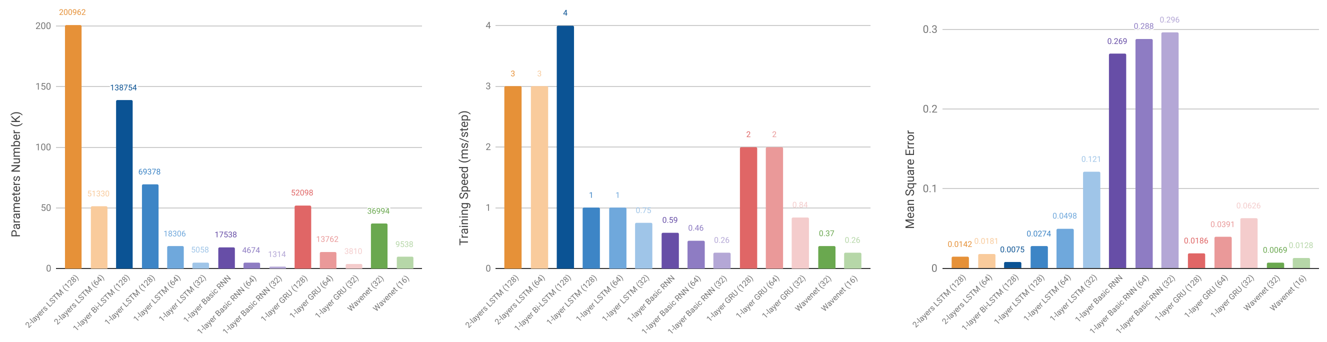

(a) (b) (c)

Fig. 5. Comparison of IONet and L-IONet models in terms of their: (a) number of parameters, (b) training (convergence) speed, and (c) test accuracy. L-IONet shows competitive performance to IONet, but requires less memory and a quicker training time.

TABLE IV
EXECUTION TIME (MS) OF THE DNNS MODELS ON THE LOW-END DEVICES

Models	Huawei Mate 8	Nexus 5	HTC One M8	Sony SW2
2-layers LSTM (128)	38.13	38.65	88.13	342.61
2-layers LSTM (64)	11.42	14.74	33.62	109.41
1-layer Bi-LSTM (128)	27.23	31.08	71.02	261.08
1-layer LSTM (128)	12.7	16.15	37.38	130.85
1-layer LSTM (64)	4.65	7.08	16.69	48.9
1-layer LSTM (32)	1.32	2.25	3.49	18.7
1-layer Basic RNN (128)	2.4	3.13	4.63	31.2
1-layer Basic RNN (64)	0.86	1.7	2.69	14.06
1-layer Basic RNN (32)	0.46	1.13	1.94	8.78
1-layer GRU (128)	7.29	12.92	14.72	81.8
1-layer GRU (64)	3.02	6.21	8.00	35.03
1-layer GRU (32)	1.76	4.24	5.68	21.54
WaveNet (32)	3.7	6.47	13.74	56.78
WaveNet (16)	1.27	3.58	8.43	27

WaveNet (32) is around ten times faster than IONet with 1-layer Bi-LSTM when training on a Tesla K80 GPU. This indicates that L-IONet shows a competitive performance in accuracy over IONet, while still superior in the speed and resource consumption.

Table IV illustrates the execution time of different IONet (LSTM, GRU, Basic RNN) and L-IONet (WaveNet) models when deployed on Huawei Mate 8, Nexus 5, HTC One M8, and Sony SW2, respectively. The execution time (milliseconds) is the average inference time of these models at the low-end devices. The L-IONet models, i.e., WaveNet (32) and WaveNet (16), performed faster inference than the LSTM-based IONet models. Even at the smartwatch device equipped with very limited CPU and memory, our proposed L-IONet is capable of realizing real-time inference, producing outputs within only 56.78 ms [WaveNet (32)] and 27 ms [WaveNet (16)] for each step. The inference speed of IONet with 1-layer LSTM (64) is similar to WaveNet (32), but its prediction error is almost eight times higher than WaveNet (32). We further compare LSTM (32) with WaveNet (32) and find that the prediction error of LSTM (32) increases to 17.5 times higher than WaveNet (32), although LSTM (32) is with faster inference speed. It is interesting to see that GRUs are more lightweight compared with both LSTM and WaveNet models. However, the prediction accuracy of GRU models are not satisfying with larger prediction errors, i.e., 0.0186, 0.0391, and 0.0626 for GRU(128), GRU(64), and GRU (32), respectively, around 3, 6, and 9 times higher than WaveNet (32). The basic RNNs (128) (64) (32) have fewer parameters, and faster inference speed on low-end devices than our WaveNet-based L-IONet, but they almost learned nothing from inertial data with huge test errors (i.e., 0.268, 0.288, and 0.296), nearly 40 times larger than the WaveNet models. Therefore, our WaveNet-based L-IONet models show better tradeoff between the prediction accuracy and on-device inference efficiency. It is worth noticing that the Wavenet-based L-IONet owns the advantages of faster training speed over Basic RNNs, LSTMs, and GRUs, as shown in Fig. 5(b). This is because the feed-forward models are easier to train and optimize than recurrent models.

C. Velocity and Heading Estimation

As a demonstration of training performance, the IONet and L-IONet models were trained on the OxIOD data set to predict the average velocity and heading rate of pedestrian motion. The average velocity $\bar{v}$ and heading rate $\dot{\psi}$ are defined as the location displacement Δl and heading change $\Delta\psi$ during a window size of time n

$$(\bar{v}, \dot{\psi}) = (\Delta l/n, \Delta\psi/n). \tag{7}$$

In our experiment setup, the window size n was chosen as 2 s, so a sequence of inertial data (200 frames) $(\{(\mathbf{a}_i, \mathbf{w}_i)\}_{i=1}^{n})$ is fed into IONet or L-IONet model to predict the average velocity $\bar{v}$ and heading rate $\dot{\psi}$

$$\left(\bar{v}, \dot{\psi}\right) = \text{IONet or L-IONet}\left(\{(\mathbf{a}_i, \mathbf{w}_i)\}_{i=1}^{n}\right) \tag{8}$$

where we used IONet with 1-layer 128-D bidirectional LSTM, and L-IONet with 32-filters WaveNet for training and prediction.

The training data are from the training sets of three motion modes categories: 1) walking normally (handheld, 20 sequences); 2) walking slowly (7 sequences); and 3) running (6 sequences). To test its generalization ability, we performed randomly walking in the Vicon room, and used the trained neural network to predict the values for selected three motion modes and a mix of activities, respectively. Fig. 6 indicates that both IONet and L-IONet can model a variety of complex motions, and generalize well to mixed activities. The more

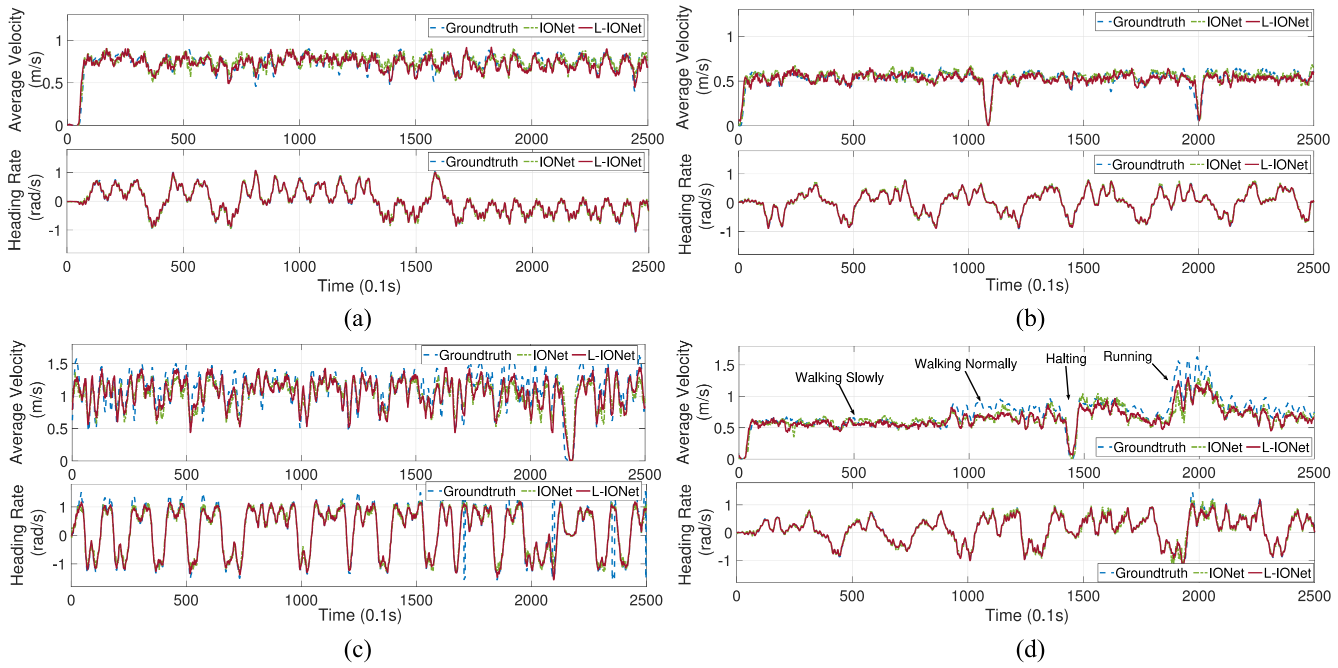

Fig. 6. Velocity and heading estimations for: (a) walking normally, (b) walking slowly, (c) running, and (d) mixed motion modes. The ground truth was captured by Vicon system, while the values from IONet and L-IONet were predicted by the learning model trained on our proposed data set.

lightweight L-IONet does not suffer an accuracy loss in this task.

D. Deep-Learning-Based Pedestrian Inertial Navigation

We show how to solve the pedestrian inertial navigation problem using DNNs with the aid of our proposed OxIOD data set. IONet and L-IONet models can reconstruct trajectories from raw IMU data, and provide users with their accurate locations. A 1-layer bidirectional LSTM with 128-D hidden states was adopted for IONet, while the WaveNet with 32 filters was used in L-IONet for the evaluation. Both models were trained with the above detailed split training sets from the four attachment categories, i.e., the handheld (20 sequences), pocket (10 sequences), handbag (7 sequences), and trolley (12 sequences). Two sets of experiments were conducted to evaluate our proposed models.

The first set of tests involved tracking a pedestrian with the phone in different attachments. In this experiment, the participant carrying the smartphone was asked to walk normally inside the Vicon room. The IMU data[2] were collected and fed into the IONet and L-IONet to predict the participant's motion. The installed motion capture systems can provide highly precise trajectories as ground truth. Note that these walking trajectories are not present in the training data set. A basic PDR algorithm was implemented as a baseline, and we show that our data set can also be used as a benchmark for conventional PDR algorithms. Fig. 7 demonstrates the trajectories generated from the ground truth (blue line), PDR (green line), IONet (orange line), and L-IONet (red line). It indicates that the deep-learning-based methods outperformed the model-based PDR when the phone was placed either in the hand, pocket or handbag. The trolley tracking is a difficult problem for PDR algorithms, as no step (periodicity pattern) can be detected in this case, and hence a handcrafted model is hard to build for this wheeled motion. In contrast, the learning-based approaches are still able to generalize to this general motion, and reconstruct physically meaningful trajectories, while the PDR algorithm fails in this task. The L-IONet model produced results even closer to the ground truth compared with IONet, especially in the handheld and trolley domains. Fig. 7(b) indicates that the IONet shows better performance when mobile device is inside pocket. This is because inertial sensor experiences less motion-dynamics inside pocket (pocket can be viewed to constrain mobile device when users are moving), so that LSTM-based IONet is already good enough to capture its self-motion from inertial data. In the other domains, the WaveNet-based L-IONet is more capable of representing the free motion of sensor, due to the expressive capability of WaveNet in processing long sequential data.

The other set of experiments is to perform large-scale localization on two floors of an office building. Although DNN models were trained with inertial data collected inside the Vicon room, we show that the models can be used to predict the pedestrian motion outside the room directly. This is due to the fact that inertial data are not sensible to environments, and hence the proposed DNN models can generalize to new environment easily. Fig. 8 demonstrates that both IONet and L-IONet models achieve good localization results, although the two models never saw any data outside the Vicon room. This experiment shows the generalization ability of the deep-learning-based models toward new environments.

[2]The test data can be found at the "test" fold of our data set.

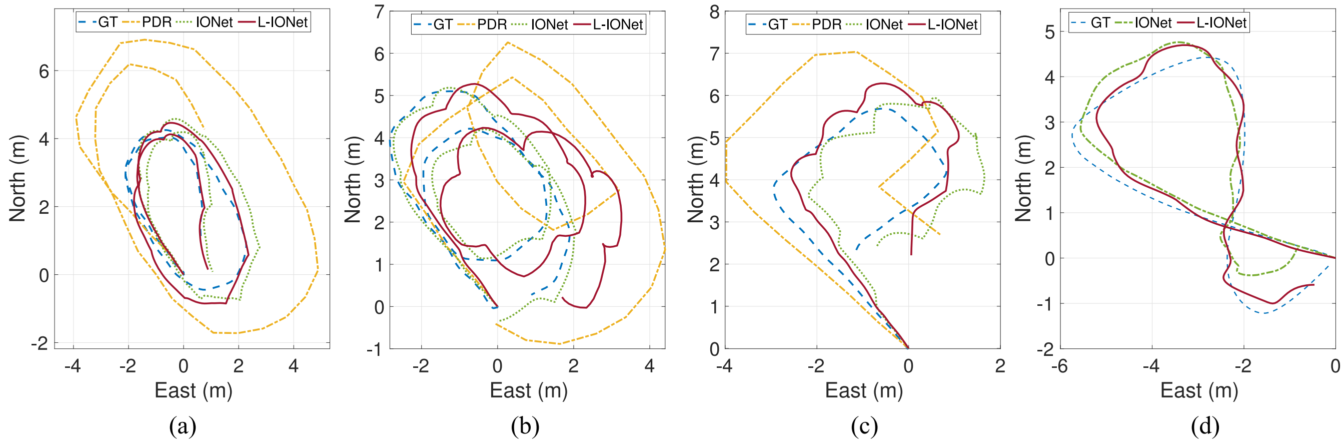

Fig. 7. Trajectories reconstruction for pedestrian tracking with device in four attachments: (a) in the hand, (b) in the pocket, (c)in the handbag, and (d) on the trolley, respectively. The trajectories were generated from IONet, L-IONet, and a basic PDR algorithm. PDRs do not work when the device was placed on the trolley, as no step can be detected in this situation. The ground truth values are provided by the Vicon System.

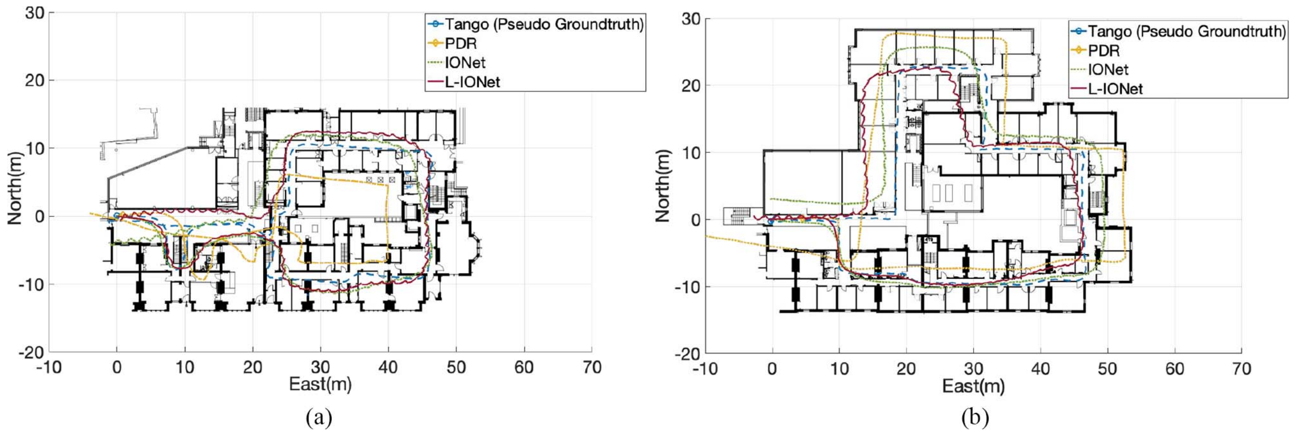

Fig. 8. Large-scale localization experiments were conducted on: (a) office floor 1 and (b) office floor 2. The trajectories were generated from the IONet, L-IONet, and PDR. The pseudo ground truth was provided by Google Tango device.

VI. Conclusion

In this article, we proposed L-IONet, a lightweight DNNs framework to learn inertial tracking from raw IMU data. L-IONet shows competitive performance over previous deep inertial odometry models. Meanwhile, L-IONet is more efficient in memory, inference, and training. We conducted a systematic research into the performance of deep-learning-based inertial odometry models on low-end devices. Our L-IONet is able to achieve a real-time inference on different levels of smartphones, and even the smartwatch with very limited computational resources. Moreover, we presented and released OxIOD, an inertial odometry data set for training and evaluating the inertial navigation models. With the release of this large-scale diverse data set, it is our hope that it will prove valuable to the community and enable future research in long-term ubiquitous ego-motion estimation.

Future work would include collecting data from more challenging situations, for example, 3-D tracking. We plan to create online common benchmark and tools for the comparison of odometry models. We also hope to include more IoT devices into our data set, such as smartwatch, wristband, and smart earphones, to extend the potential applications of this research. A further extension to the current deep inertial odometry models is to adopt knowledge distillation to compress the DNNs, which can reduce the number of parameters and enable faster training and on-device inference. Another future research direction is to investigate how to formulate dilated casual convolutional model (i.e., WaveNet style model) as a generic framework to process a variety of sensor data, e.g., temperature, pressure, light intensity, and magnetic field, in other potential IoT application domains, e.g., health/activity monitoring, sport analysis, smart home, and intelligent transportation. Except the DNNs discussed above, other machine learning models might also be applied into data-driven IoT research domains, for example, deep belief network (DBN) or broad learning system (BLS).

References

[1] R. Harle, “A survey of indoor inertial positioning systems for pedestrians,” *IEEE Commun. Surveys Tuts.*, vol. 15, no. 3, pp. 1281–1293, 3rd Quart., 2013.

[2] M. Gowda *et al.*, “Bringing IoT to sports analytics,” in *Proc. NSDI*, 2017, pp. 499–513.

[3] V. Bianchi, M. Bassoli, G. Lombardo, P. Fornacciari, and M. Mordonini, "IoT wearable sensor and deep learning: An integrated approach for personalized human activity recognition in a smart home environment," *IEEE Internet Things J.*, vol. 6, no. 5, pp. 8553–8562, Oct. 2019.

[4] E. Marchand, H. Uchiyama, and F. Spindler, "Pose estimation for augmented reality: A hands-on survey," *IEEE Trans. Vis. Comput. Graphics*, vol. 22, no. 12, pp. 2633–2651, Dec. 2016.

[5] S. Leutenegger, S. Lynen, M. Bosse, R. Siegwart, and P. Furgale, "Keyframe-based visual-inertial odometry using nonlinear optimization," *Int. J. Robot. Res.*, vol. 34, no. 3, pp. 314–334, 2015.

[6] S. Kuutti, S. Fallah, K. Katsaros, M. Dianati, F. Mccullough, and A. Mouzakitis, "A survey of the state-of-the-art localization techniques and their potentials for autonomous vehicle applications," *IEEE Internet Things J.*, vol. 5, no. 2, pp. 829–846, Apr. 2018.

[7] N. El-Sheimy, H. Hou, and X. Niu, "Analysis and modeling of inertial sensors using allan variance," *IEEE Trans. Instrum. Meas.*, vol. 57, no. 1, pp. 140–149, Jan. 2008.

[8] J.-O. Nilsson, I. Skog, P. Händel, and K. V. S. Hari, "Foot-mounted INS for everybody—An open-source embedded implementation," in *Proc. IEEE Position Location Navig. Symp. (PLANS)*, 2012, pp. 140–145.

[9] C. Chen, X. Lu, A. Markham, and N. Trigoni, "IONet: Learning to cure the curse of drift in inertial odometry," in *Proc. 32nd AAAI Conf. Artif. Intell.*, New Orleans, LA, USA, Feb. 2018, pp. 6468–6476.

[10] H. Yan, Q. Shan, and Y. Furukawa, "RIDI: Robust IMU double integration," in *Proc. Eur. Conf. Comput. Vis.*, 2018, pp. 1–16.

[11] S. Cortés, A. Solin, and J. Kannala, "Deep learning based speed estimation for constraining strapdown inertial navigation on smartphones," 2018. [Online]. Available: http://arxiv.org/abs/1808.03485.

[12] A. Geiger, P. Lenz, C. Stiller, and R. Urtasun, "Vision meets robotics: The KITTI data set," *Int. J. Robot. Res.*, vol. 32, no. 11, pp. 1231–1237, 2013.

[13] W. Maddern, G. Pascoe, C. Linegar, and P. Newman, "1 year, 1000km: The Oxford robotcar data set," *Int. J. Robot. Res. (IJRR)*, vol. 36, no. 1, pp. 3–15, 2016.

[14] D. Schubert, T. Goll, N. Demmel, V. Usenko, J. Stückler, and D. Cremers, "The TUM VI benchmark for evaluating visual-inertial odometry," in *Proc. IEEE/RSJ Int. Conf. Intell. Robots Syst. (IROS)*, 2018, pp. 1680–1687.

[15] S. Cortés, A. Solin, E. Rahtu, and J. Kannala, "ADVIO: An authentic data set for visual-inertial odometry," in *Proc. Eur. Conf. Comput. Vis. (ECCV)*, 2018, pp. 425–440.

[16] F. Samie, L. Bauer, and J. Henkel, "From cloud down to things: An overview of machine learning in Internet of Things," *IEEE Internet Things J.*, vol. 6, no. 3, pp. 4921–4934, Jun. 2019.

[17] M. Burri *et al.*, "The EuRoC micro aerial vehicle data sets," *Int. J. Robot. Res.*, vol. 35, no. 10, pp. 1157–1163, 2016.

[18] M. Zhang and A. A. Sawchuk, "USC-HAD: A daily activity data set for ubiquitous activity recognition using wearable sensors," in *Proc. ACM Conf. Ubiquitous Comput. (UbiComp)*, 2012, pp. 1036–1043.

[19] F. De La Torre *et al.*, "Guide to the Carnegie mellon university multimodal activity (CMU-MMAC) database," Robot. Inst., Carnegie Mellon Univ., Pittsburgh, PA, USA, Rep. CMU-RI-TR-08-22, Apr. 2008.

[20] R. Chavarriaga *et al.*, "The opportunity challenge: A benchmark database for on-body sensor-based activity recognition," *Pattern Recognit. Lett.*, vol. 34, no. 15, pp. 2033–2042, 2013.

[21] S. Khandelwal and N. Wickström, "Evaluation of the performance of accelerometer-based gait event detection algorithms in different real-world scenarios using the MAREA gait database," *Gait Posture*, vol. 51, pp. 84–90, Jan. 2017.

[22] D. Chen *et al.*, "Smart insole-based indoor localization system for Internet of Things applications," *IEEE Internet Things J.*, vol. 6, no. 4, pp. 7253–7265, Aug. 2019.

[23] Y. Zhuang, J. Yang, L. Qi, Y. Li, Y. Cao, and N. El-sheimy, "A pervasive integration platform of low-cost MEMS sensors and wireless signals for indoor localization," *IEEE Internet Things J.*, vol. 5, no. 6, pp. 4616–4631, Dec. 2018.

[24] Y. Li, Z. He, Z. Gao, Y. Zhuang, C. Shi, and N. El-Sheimy, "Toward robust crowdsourcing-based localization: A fingerprinting accuracy indicator enhanced wireless/magnetic/inertial integration approach," *IEEE Internet Things J.*, vol. 6, no. 2, pp. 3585–3600, Apr. 2019.

[25] S. Wang, H. Wen, R. Clark, and N. Trigoni, "Keyframe based large-scale indoor localisation using geomagnetic field and motion pattern," in *Proc. IEEE/RSJ Int. Conf. Intell. Robots Syst. (IROS)*, 2016, pp. 1910–1917.

[26] R. Liu, C. Yuen, T.-N. Do, D. Jiao, X. Liu, and U.-X. Tan, "Cooperative relative positioning of mobile users by fusing IMU inertial and UWB ranging information," in *Proc. IEEE Int. Conf. Robot. Autom. (ICRA)*, Singapore, May/Jun. 2017, pp. 5623–5629.

[27] B. Wagstaff and J. Kelly, "LSTM-based zero-velocity detection for robust inertial navigation," in *Proc. Int. Conf. Indoor Position. Indoor Navig. (IPIN)*, Sep. 2018, pp. 24–27.

[28] *Vicon Motion Capture Systems: Viconn*, Vicon, Hauppauge, NY, USA, 2017.

[29] *Google Tango Tablet*, Tango, St Petersburg, Russia, 2014. [Online]. Available: https://get.google.com/tango/

[30] Z. Xiao, H. Wen, A. Markham, and N. Trigoni, "Robust pedestrian dead reckoning (R-PDR) for arbitrary mobile device placement," in *Proc. Int. Conf. Indoor Position. Indoor Navig. (IPIN)*, 2014, pp. 187–196.

[31] H. Weinberg, *Using the ADXL202 in Pedometer and Personal Navigation Applications*, Analog Devices, Norwood, MA, USA, 2002.

[32] S. Yao *et al.*, "FastDeepIoT: Towards understanding and optimizing neural network execution time on mobile and embedded devices," in *Proc. 16th ACM Conf. Embedded Netw. Sensor Syst. (SenSys)*, 2018, pp. 278–291.

[33] K. Greff, R. K. Srivastava, J. Koutník, B. R. Steunebrink, and J. Schmidhuber, "Lstm: A search space odyssey," *IEEE Trans. Neural Netw. Learn. Syst.*, vol. 28, no. 10, pp. 2222–2232, Oct. 2017.

[34] A. van den Oord *et al.*, "WaveNet: A generative model for raw audio," 2016. [Online]. Available: arXiv:1609.03499.

[35] F. Yu and V. Koltun, "Multi-scale context aggregation by dilated convolutions," in *Proc. Int. Conf. Learn. Represent. (ICLR)*, 2016, pp. 1–13.

[36] A. Vaswani *et al.*, "Attention is all you need," in *Proc. Adv. Neural Inf. Process. Syst.*, 2017, pp. 5998–6008.

[37] J. Devlin, M.-W. Chang, K. Lee, and K. Toutanova, "Bert: Pre-training of deep bidirectional transformers for language understanding," in *Proc. Conf. North Amer. Ch. Assoc. Comput. Linguist. Human Lang. Technol.*, vol. 1, 2019, pp. 4171–4186.

[38] D. P. Kingma and J. Ba, "Adam: A method for stochastic optimization," in *Proc. Int. Conf. Learn. Represent. (ICLR)*, 2015, pp. 1–15.